



Design, synthesis and computational studies involving Indole-Coumarin hybrids as galectin-1 inhibitors

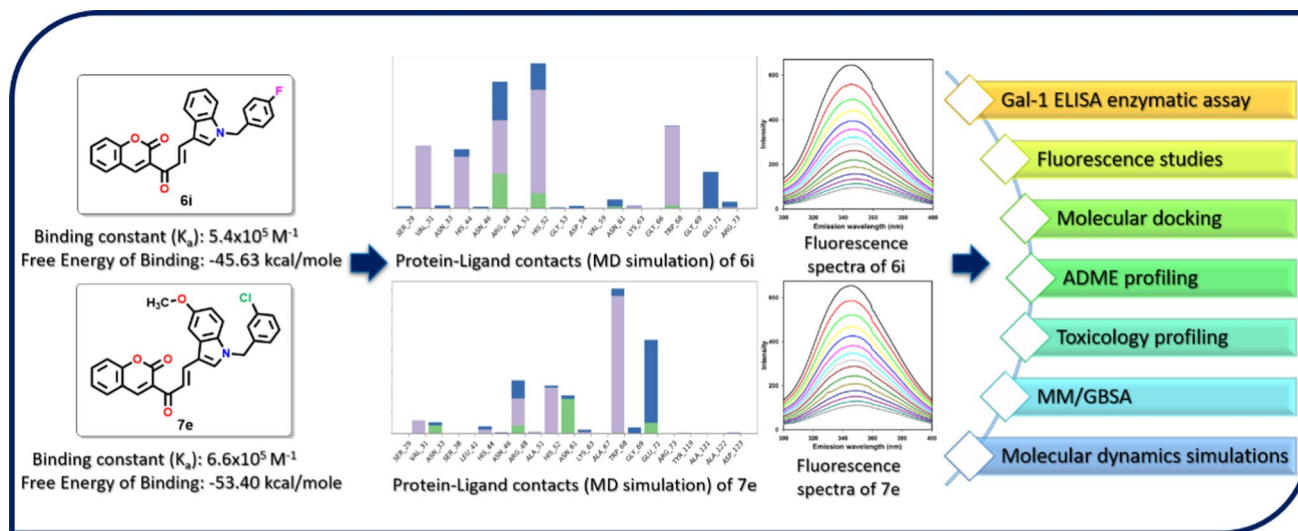
Aaftaab Sethi¹ · K. Sasikala¹ · Pranay Jakkula² · Divya Gadde³ · Swetha Sanam¹ · Insaf A. Qureshi² · Venu Talla³ · Mallika Alvala^{1,4}

Received: 19 November 2020 / Accepted: 21 January 2021 / Published online: 2 February 2021
© Institute of Chemistry, Slovak Academy of Sciences 2021

Abstract

In continuation of our quest to develop non-carbohydrate galectin-1 inhibitors, we have designed and synthesized 20 indole-coumarin hybrids linked via chalcone. Compounds **6i** and **7e** were found to decrease galectin-1 levels significantly in galectin-1 enzyme assay at 20 μM concentration. Binding affinity studies carried out by fluorescence spectroscopy revealed that **6i** binds to galectin-1 with a binding constant (K_a) value of $5.4 \times 10^5 \text{ M}^{-1}$ while **7e** was found to have a slightly higher affinity than **6i** with K_a of $6.6 \times 10^5 \text{ M}^{-1}$. Molecular docking was carried out to ascertain the interaction between ligand and protein. To further gain structural insights into the binding of the compounds, 30 ns molecular dynamic simulations were carried out. The studies revealed that compound **7e** was stable within the subsite C of galectin carbohydrate recognition domain while **6i** fluctuated throughout the simulation. In addition, **7e** maintained continuous interaction with Trp68 and His52, the two key amino acid residues are responsible for recognition of ligands within the active site. Furthermore, **7e** displayed H-bond interactions with highly conserved amino acids within galectin-1 CRD, i.e., Arg48, Asn61 and Glu71. Free energy of binding evaluated by MM-GBSA calculations was also in accordance with experimental data. **7e** was calculated to have binding energy of -53.40 kcal/mole while **6i** was found to have a value of -45.63 kcal/mole .

Graphical abstract



Keywords Galectins · Galectin-1 · Gal-1 inhibitors · Non-carbohydrate inhibitors · Indole-coumarin hybrids · Chalcones

✉ Mallika Alvala
mallikaalvala@yahoo.in

Extended author information available on the last page of the article

Introduction

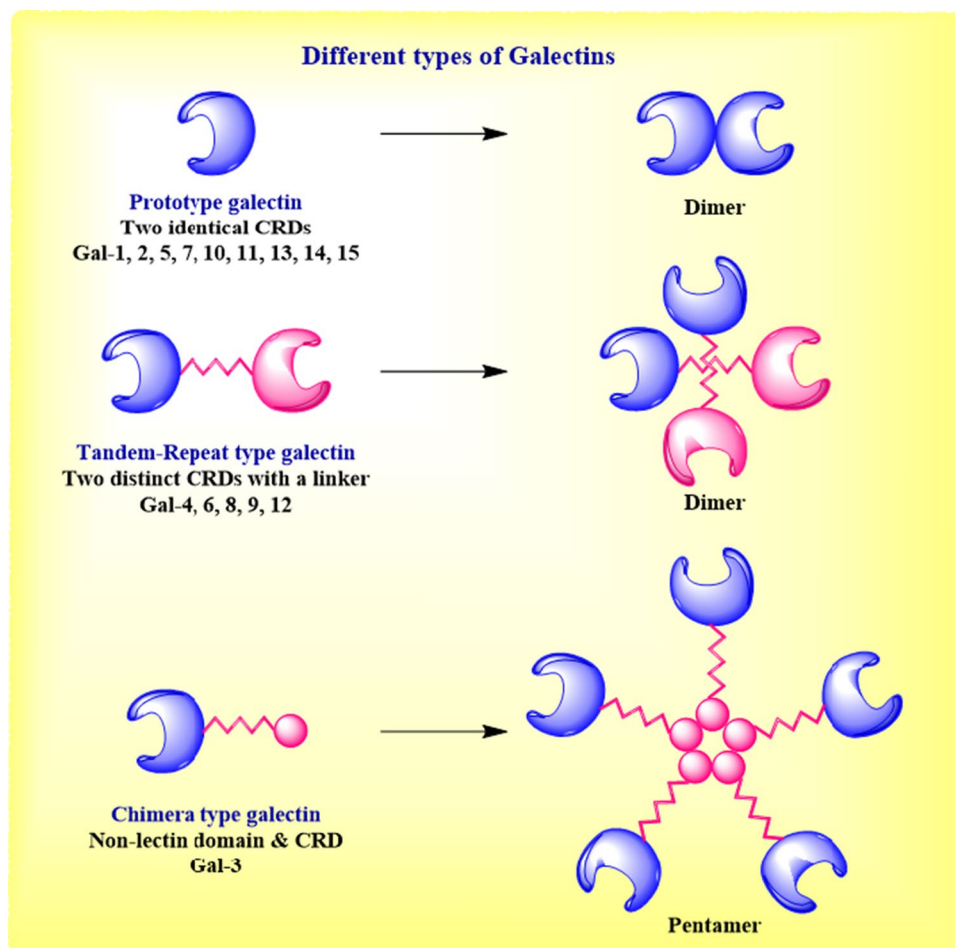
Galectins are proteins that belong to the family of lectins and bind specially to the β -galactoside containing glycans. They are characterized by the presence of conserved amino acid sequence motifs (130–140 amino acids) in their carbohydrate-binding sites known as carbohydrate recognition domain (CRD) (Barondes et al. 1994). In total, 15 galectins have been reported till date and they are classified into three types, namely, prototype galectins (galectin-1, -2, -5, -7, -10, -11, -13, -14, and -15), tandem-repeat galectins (galectin-4, -6, -8, -9, and -12) and chimera galectin (galectin-3) based on their structural organization (Fig. 1) (Leffler et al. 2002).

Galectin-1 (Gal-1) is a highly conserved protein with a single CRD composed of 135 amino acids. Its expression is ubiquitous inside our body in normal tissues and diseased ones (Hughes 1999; Cooper and Barondes 1990). It regulates cell growth, cell development, cell differentiation, cell adhesion, signaling and immune system (Liu et al. 2002; Patterson et al. 2004; He and Baum 2006). The altered Gal-1 expression is associated with various

pathological conditions related to neurological diseases (Wada et al. 2003), HIV-1 viral infection (Mercier et al. 2008) tumor progression (prostate, thyroid, bladder and ovary), carcinomas, astrocytoma and melanoma (Rabinovich 2005). Gal-1 is also a diagnostic tumor marker (Thijssen et al. 2015). Thus, due to its ubiquitous expression and wide range of activities, Gal-1 has emerged as a potential therapeutic target for the treatment of a variety of disease conditions like neurodegeneration, inflammation, cancer and viral infection (Sundblad et al. 2017; Sethi et al. 2020).

Majority of Gal-1 inhibitors reported till date are carbohydrates or carbohydrate derivatives. However, this class of inhibitors has certain drawbacks. The synthesis and characterization of carbohydrate-based inhibitors is challenging, expensive and requires extensive protecting group alteration (Boltje et al. 2009). Moreover, they are unable to cross the cell membrane and aren't selective. Similarly, peptide-based inhibitors of Gal-1 also face challenges such as high cost and poor bioavailability (Blanchard et al. 2016). One excellent substitute to these class of compounds is heterocyclic molecules as Gal-1 inhibitors. The heterocyclic compounds' properties can be easily tinkered with, as structural

Fig. 1 Representative structures of different isoforms of Galectin



modifications on these systems are rather easy (Gomtsyan 2012). The literature involved regarding synthetic methods for developing these molecules is large and well established. Very recently, there have been a few reports of heterocyclic molecules as galectin inhibitors by our research group and others (Goud et al. 2019a, b, 2020; Gabr et al. 2020). In continuation of our pursuit to develop non-carbohydrate Gal-1 inhibitors, herein, we report synthesis of 20 indole-coumarin hybrids as Gal-1 inhibitors. There was extensive literature supporting the rationale to choose these hybrids. Coumarin scaffold has been utilized previously on many occasions as Gal-1 inhibitor. Rajput et al. have reported use of coumarin on two separate occasions to develop Gal-1 inhibitors. **I** and **II** with K_d value of 1900 and 16 μM , respectively (Rajput et al. 2014, 2016). Goud et al. (2019a, b; 2020) reported a coumarin thiazole derivative as Gal-1 inhibitor (**III**) with a binding constant (K_a) of $1.9 \times 10^7 \text{ M}^{-1}$ and in another article reported a 4,7-disubstituted coumarin (**IV**) with K_a $1.3 \times 10^4 \text{ M}^{-1}$. The same group also reported 1-benzyl-1H-benzimidazoles (**V**) as Gal-1 inhibitor with $K_a = 1.2 \times 10^4 \text{ M}^{-1}$ (Goud et al. 2019a, b). Indole is yet another decorated scaffold in medicinal chemistry. It is the 9th most common nitrogen heterocycle found in US FDA-approved drugs (Vitaku et al. 2014). Biological importance of indoles is vast and ranges from anti-microbial, anti-tumor, anti-inflammatory, anti-oxidant, anti-viral, anti-cancer and anti-parkinsonian among others (Sraavanthi and Manju 2016). But naturally, indoles have also found their way as galectin inhibitors. Tejler et al. (2005) reported anomeric aldoxime derivatives of β -galactose as Gal-3 inhibitors. They found that three of the best inhibitors consisted of a bicyclic aromatic moiety in form of naphthalene, quinoline and indole. Among them, indole derivative was found to be the most potent inhibitor (**VI**) with K_d of 180 μM . The same group in another subsequent study reported inhibitor **VII** with a K_d value of 46 μM toward Gal-3 (Tejler et al. 2009). Consequently, along these lines, we decided to design indole-coumarin hybrids as potential Gal-1 inhibitor. The galectin CRD is considerably big and thus we wanted an appropriately sized linker which in itself is biologically active and does not adapt many conformations. Michael acceptors containing an electrophile are considered biologically active as such motifs can react with biological molecules and bind with them (Zhuang et al. 2017). Keeping this in mind, chalcone was chosen for the role of the linker. Chalcones possess biological potency for a wide variety of diseases. Chalcones like metochalcone (**VIII**) and sofalcone (**IX**) have also found their way into clinical practice (Gomes et al. 2017). Kurt et al. (2020) designed coumarin-chalcone derivatives (**X**) among which one of them was reported to have better anti-cancer activity on H4IIE cancer cell line when compared to the reference drug Sorafenib. The summary of the rationale of designed molecules is illustrated in Fig. 2.

Results and discussion

Chemistry

The target compounds **6a–n** and **7a–f** were synthesized in 3 steps (Scheme 1). Initially, Knoevenagel condensation between aldehydic functionality of salicylaldehyde (**1**) and active methylene of ethylacetoacetate (**2**) in presence of piperidine followed by cyclization gave us 3-acetyl coumarin (**3**) in high yields. Next, we made use of Claisen–Schmidt condensation between (**3**) and substituted indole carbaldehyde (**4**) to give us chalcone (**5**) in good yield. Finally, we carried out a simple nucleophilic substitution reaction between alkyl/aryl halides and (**5**) which gave us the target compound N-substituted indole-coumarin hybrids in moderate-to-excellent yields. All the newly synthesized compounds **6a–n** and **7a–f** (Fig. 3) were characterized by HRMS, ^1H , and ^{13}C NMR spectroscopy. The alkene protons part of the chalcone consistently showed a coupling constant of $> 15 \text{ Hz}$ in ^1H NMR spectrum of the compounds confirming that the E(trans) isomer was formed, which is also the predominant stereoisomer (Gomes et al. 2017). The ^1H NMR spectrum of the compounds containing CH_2 benzylic protons displayed a sharp singlet between $\delta 5\text{--}6$. The ^{13}C NMR spectrum displayed the characteristic peak of carbonyl carbon of chalcone at $> \delta 180$. The benzylic carbon was also observed in ^{13}C NMR spectrum of the compounds in the range of $\delta 40\text{--}60$ as a singlet except for compounds wherein a fluoro group at the ortho position is present. In those cases, the benzylic proton was observed as a doublet. The HRMS (ESI) of compounds showed corresponding $[\text{M} + \text{H}]^+$ peaks based on their molecular weights.

1.1 Biological activity (enzymatic assay and fluorescence studies).

Initially, a preliminary investigation was done using an enzyme assay to ascertain the ability of the synthesized molecules **6a–n** and **7a–f** to reduce the Gal-1 expression. BT-474 cells were grown in a 12-well plate and treated with 20 μM concentration of compounds for 24 h. Then the supernatant was collected as Gal-1 is an extracellular secreted protein. Equal amounts of supernatant are subjected to Quantikine Enzyme-Linked Immunoassay (ELISA) as per manufacturer's protocol (DGAL 10, R&D systems). The supernatant was diluted twofold with calibrator diluent and incubated with human Gal-1-coated plates for 2 h at room temperature on a horizontal orbital microplate shaker and washed to remove any unbound protein. Gal-1-specific polyclonal antibody conjugated to horseradish peroxidase was added and incubated for 2 h on a shaker. It was then washed

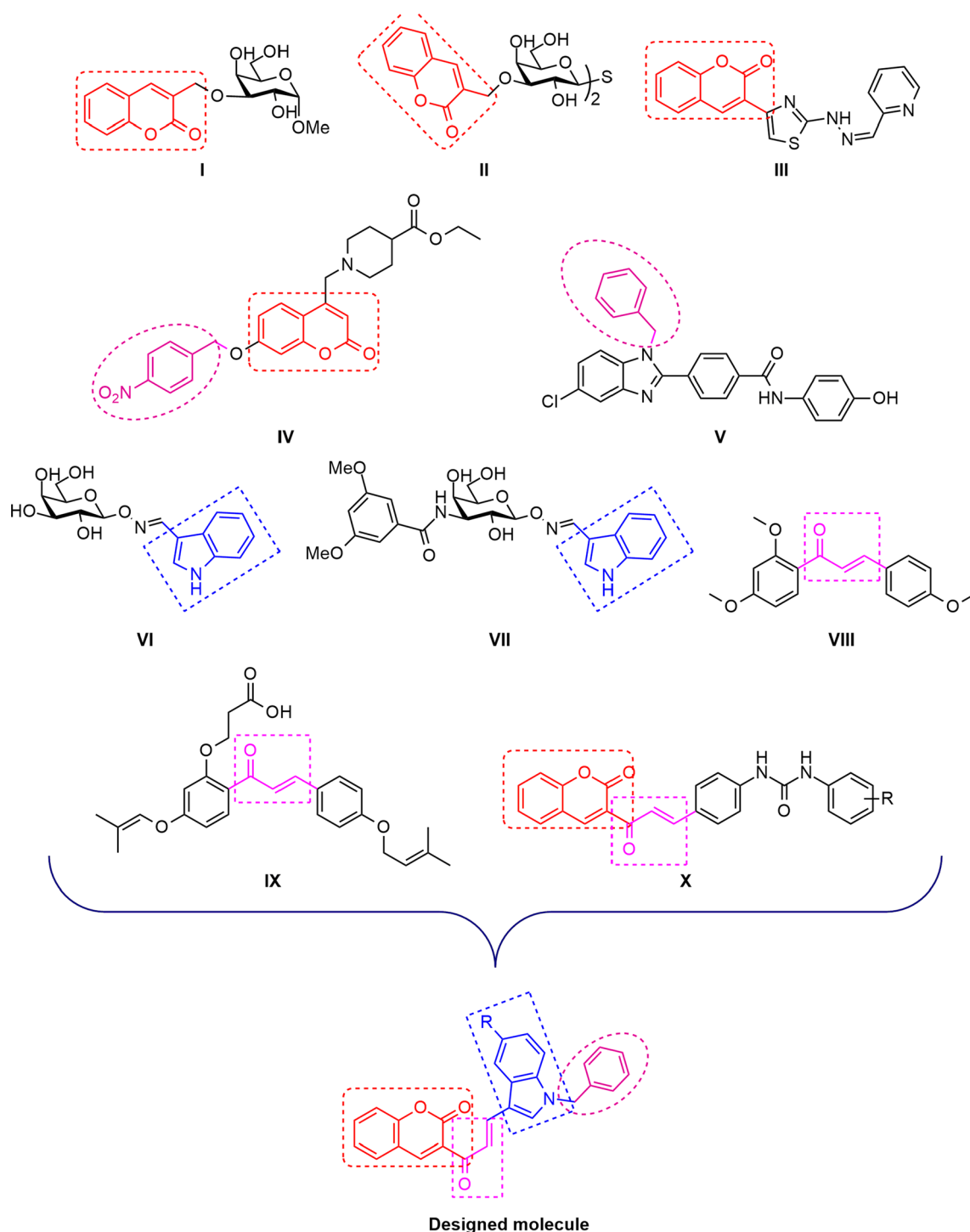
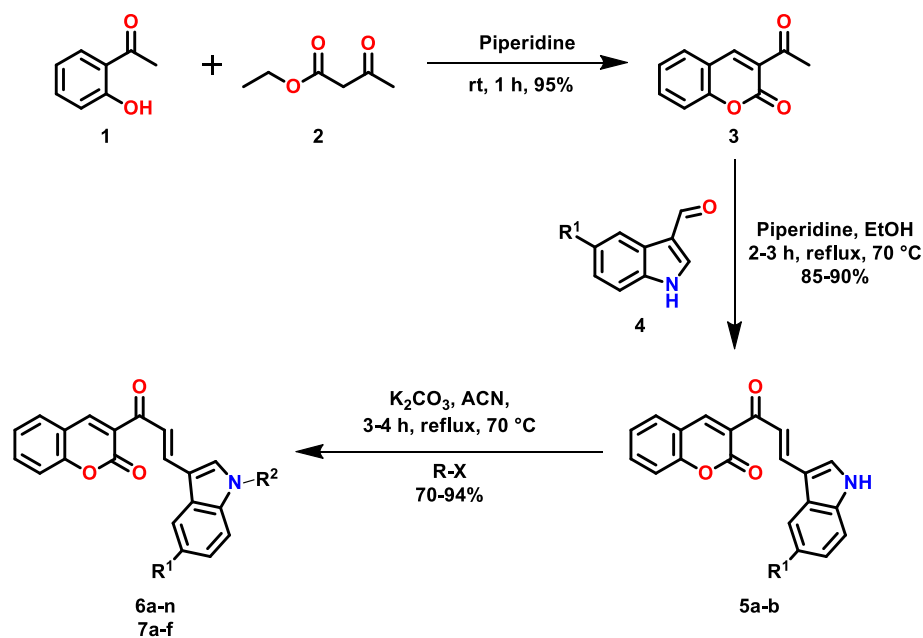
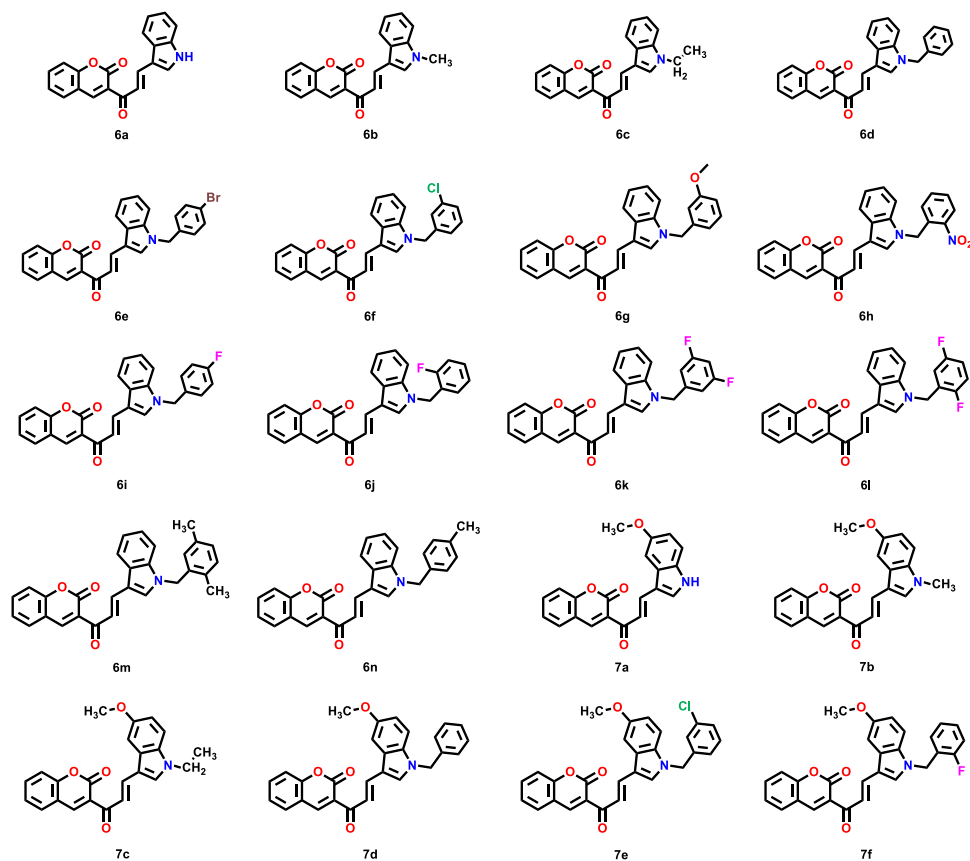


Fig. 2 Illustration highlighting the rationale behind designed molecules

and incubated with substrate solution for 30 min before terminating the reaction with 50 μ l of stop solution. Amount of protein expression was detected at 450 nm using a UV spectrophotometer. The percentage reduction of Gal-1 expression is summarized in Table 1. It was found that among all the compounds synthesized compound **6i** and **7e** significantly

reduced the Gal-1 expression. These observations are in accordance with the trend observed for Gal-1 inhibitors wherein a substitution at 3rd position of the benzyl group at the far end by fluoro or chloro substituent leads to enhanced activity as observed in the case of TD-139 and several other inhibitors (Goud et al. 2019a, b).

Scheme 1 Synthesis of indole-coumarin hybrids (**6a–n**, **7a–f**)**Fig. 3** Structure of the synthesized compounds

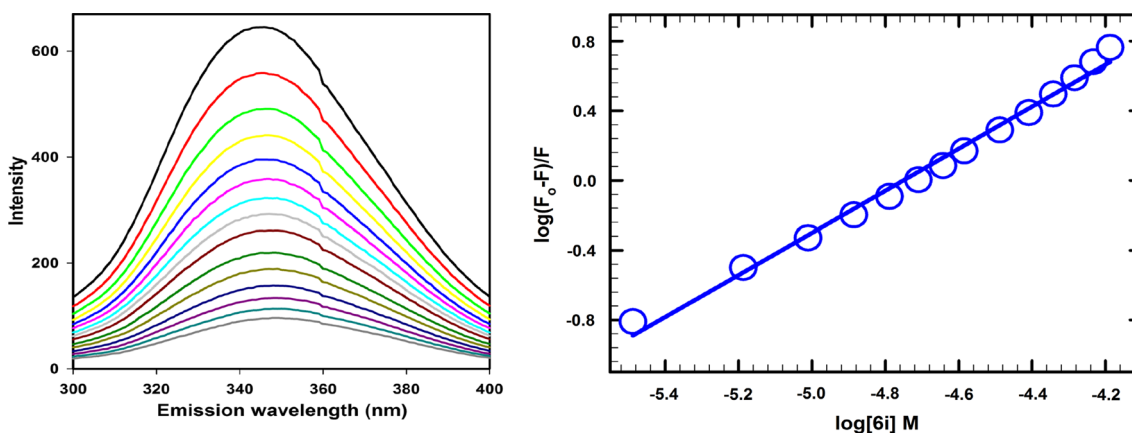
Encouraged by these results, we set out to determine the binding affinity of compounds **6i** and **7e** using fluorescence measurements. The maximum emission spectra of Gal-1 were found at 343 nm, and there was a decrease

in fluorescence intensity with increasing concentration of the compounds (Figs. 4, 5). The plot of $\log[6i]$ and $\log[7e]$ versus $\log(F_0 - F)/F$ had given a linear relationship, and the number of binding sites was calculated from the slope,

Table 1 The reduction in Gal-1 expression for synthesized compounds

Compound code	Reduction (%) 20 μ M
6a	<20
6b	<20
6c	<20
6d	<20
6e	<20
6f	<20
6g	<20
6h	<20
6i	38.68
6j	<20
6k	<20
6l	<20
6m	<20
6n	<20
7a	<20
7b	<20
7c	<20
7d	<20
7e	81.13
7f	<20

which inferred interaction of protein and compound in 1:1 ratio. The binding constant (K_d) was calculated from the intercept value which was observed as $5.4 \times 10^5 \text{ M}^{-1}$ for **6i** and $6.6 \times 10^5 \text{ M}^{-1}$ for **7e** which corroborated well with the ELISA studies. The intensity of the fluorescence was quenched upon increase of ligand concentration, and the bimolar quenching constant (K_q) was calculated to be $6.6 \times 10^{12} \text{ M}^{-1} \text{ s}^{-1}$ for **6i** and $5.9 \times 10^{12} \text{ M}^{-1} \text{ s}^{-1}$ for **7e** which is larger than diffusion control limit suggesting an interaction of protein and ligand as well as the mode of quenching to be static (Lakowicz 2013).

**Fig. 4** Fluorescence binding study of compound 6i with Gal-1

1.1 Molecular docking, molecular dynamics, MM/GBSA and ADMET studies

To understand the mode of interaction of compound **6i** and **7e** at the Gal-1 CRD, the two compounds were subjected to molecular docking. The docking was carried out using Glide module of Schrödinger suite 2020–2. The 3D crystal co-ordinates of human Gal-1 were retrieved from protein data bank (PDB ID: 4Y24). It was found that the coumarin moiety in compound **7e** was showing multiple pi-pi stacking interactions with Trp68 residue of Gal-1 protein. In addition, it displayed a H-bond interaction with Asn61 residue at a distance of 1.88 Å. On the other hand, compound **6i** displayed 2 H-bond interaction with Asn61 residue. One is shown by carbonyl of chalcone at a distance of 2.35 Å and the other by carbonyl of coumarin at a distance of 2.41 Å. However, the coumarin moiety in **6i** was tilted slightly far away from the indole ring of Trp68 due to which it was unable to show the pi-pi stacking interaction (Fig. 6). Interestingly, it has been previously reported that carbohydrate galectin recognition is characterized by a stacking interaction between the sugar ring and an aromatic residue of Trp68 (Meynier et al. 2009). Trp68 a conserved residue within the galectin family and is a key amino acid involved in recognition of galactose (Di-Lella et al. 2009). Thus, it was gratifying to find that both the compounds fit well into the Gal-1 CRD and **7e** displayed the important Trp68 pi-pi stacking interaction. The respective docking scores of **6i** and **7e** were found to be -4.195 and -4.135 .

Merely relying on the docking score is not suitable as the protein is considered to be rigid in most of the software, while the system in which protein and ligand coexist is dynamic (Sethi et al. 2019). Thus, to further understand the mode of binding, compounds **6i** and **7e** were subjected to molecular dynamics (MD) simulation of 30 ns. The MD

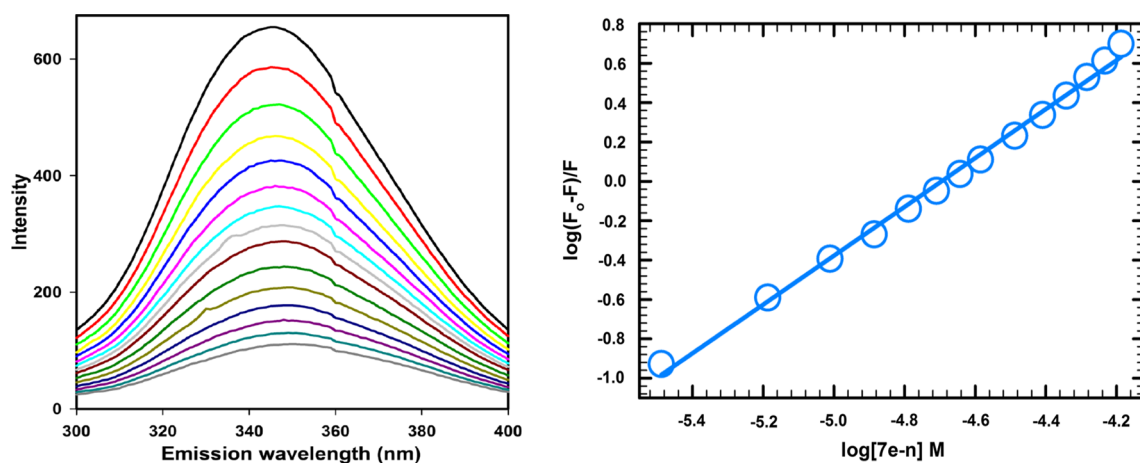


Fig. 5 Fluorescence binding study of compound **7e** with Gal-1

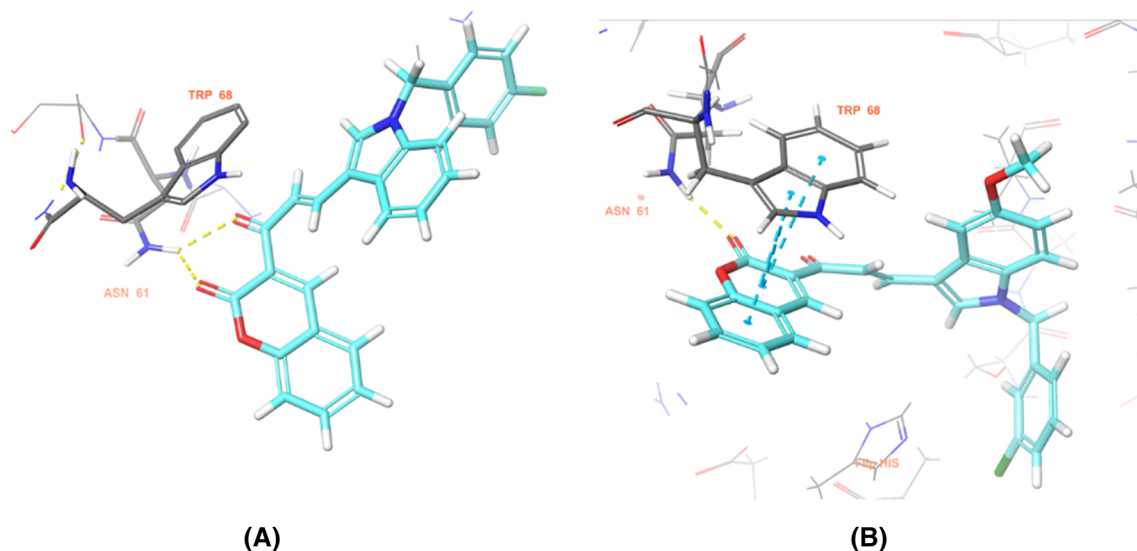


Fig. 6. 3D interaction diagram of Gal-1 protein with **a 6i** (cyan), H-bond interactions (yellow) can be observed between carbonyl oxygen of chalcone and coumarin with Asn61 residue. **b 7e** (cyan),

H-bond interaction (yellow) can be observed between carbonyl oxygen of coumarin and Asn61 residue in addition to hydrophobic interaction (blue) with Trp68

was performed using Desmond Module of Schrödinger suite 2020–2.

To understand the conformational change in the protein and ligand from its native structure the root mean square deviation (RMSD) values were analyzed (Fig. 7). Configuration RMSD for **6i** complex was first found to increase and then converge after 15 ns during equilibration phase while for **7e** complex it was found to increase as well but converge after 12 ns. Ligand **7e** fluctuated initially but was found to stabilize after 15 ns while ligand **6i** fluctuated throughout the simulation and only seemed to stabilize at the end of the simulation. Protein–ligand interactions of both the complexes were examined during the course of MD simulation.

Figure 8 demonstrates the type of protein–ligand contacts exhibited by the complexes employed in MD simulation. It was found that **6i** displayed a H-bond interaction with Arg48 and His52. Also, it displayed hydrophobic interaction with Val31, His44, Arg48, His52 and Trp68. Although the interaction with Trp68 wasn't intense, compound **7e** displayed H-bond interactions Asn61 and water bridge-mediated H-bonding with Glu71. Additionally, it exhibited a very strong hydrophobic interaction with Trp68 and relatively mild ones with Arg48 and His52. Thus, it is clear that compound **7e** was able to maintain its interactions with Asn61 and Trp68 during the course of the simulation. The simulation also demonstrated the importance of pi-pi stacking

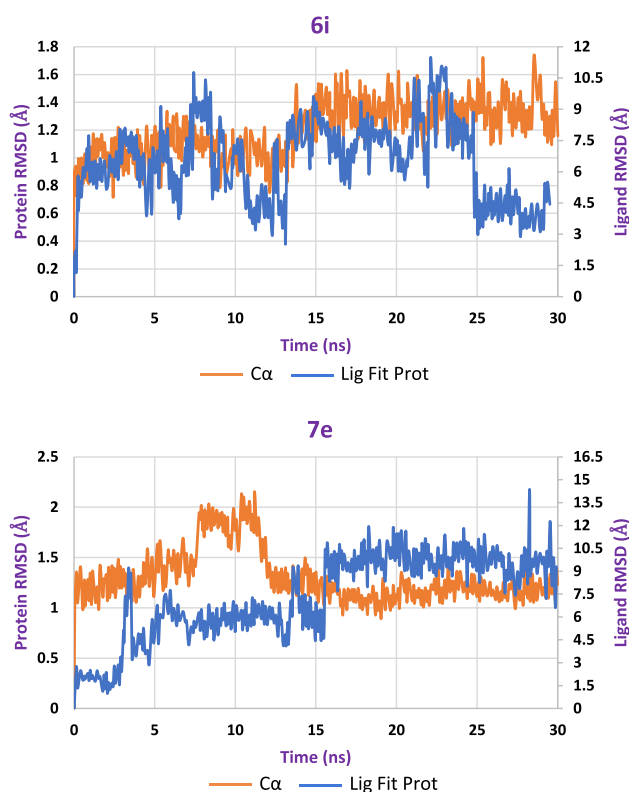


Fig. 7 Average RMSD of protein (Orange) and ligand (Blue) for Gal-1 ligand complexes **a** **6i** and **b** **7e** during molecular dynamics simulation

interaction with Trp68. Compound **7e** stabilized early while **6i** fluctuated throughout most of the simulation. The free energy of binding was calculated for the docked complexes of **6i** and **7e** using the MM/GBSA method incorporated in Prime module of Schrödinger suite 2020–2. The free energy of binding was determined to be -53.40 kcal/mole for **7e** while for **6i** it was found to be -45.63 kcal/mole. These results are in accordance with the experimental and MD simulation data.

The absorption, distribution, metabolism, excretion and toxicity (ADMET) data were evaluated for compounds **6i** and **7e** using pkCSM web server (Pires et al. 2015). **6i** was found to have a high intestinal absorption and high Caco-2 permeability and had a blood brain barrier (BBB) permeability of 0.236. This signifies its inability to cross the BBB. The effect of cytochrome P450 metabolism for CYP3A4 was positive while for CYP2D6 was found to be negative. The clearance value was found to be 0.897, and the compound was found to be non-mutagenic; however, certain degree of hepatotoxicity was predicted. **7e** was found to have a high intestinal absorption and high Caco-2 permeability too and had a blood brain barrier (BBB) permeability of 0.123. CYP2D6 inhibition was found to be negative while CYP3A4 was positive. The compound was

found to be non-mutagenic; however, certain degree of hepatotoxicity was predicted for **7e** as well.

Conclusion

In conclusion, we have synthesized a series of 20 novel indole-coumarin hybrids (**6a–n**, **7a–f**) and characterized by spectral techniques viz. $^1\text{H-NMR}$, $^{13}\text{C-NMR}$ and HRMS. Initially, all the compounds were tested for Gal-1 inhibition using enzymatic assay. The two most promising molecules (**6i** and **7e**) were further studied by fluorescence spectroscopy to determine their binding values. To understand their mode of binding, the two compounds were subjected to extensive computational studies. It was concluded that both these compounds interacted with Trp68 in Gal-1 CRD which led to their recognition inside the active site in addition to displaying H-bond network with multiple amino acids present within the Gal-1 CRD. MD studies further validated the interactions with Gal-1 residues within the CRD. In-silico toxicity profiling was carried out for both the molecules to identify any potential toxic effects. The molecules were found to have suitable ADME properties and were found to be non-mutagenic. However, they have been predicted to be hepatotoxic. This needs to be kept in mind while considering similar molecules as clinical candidates.

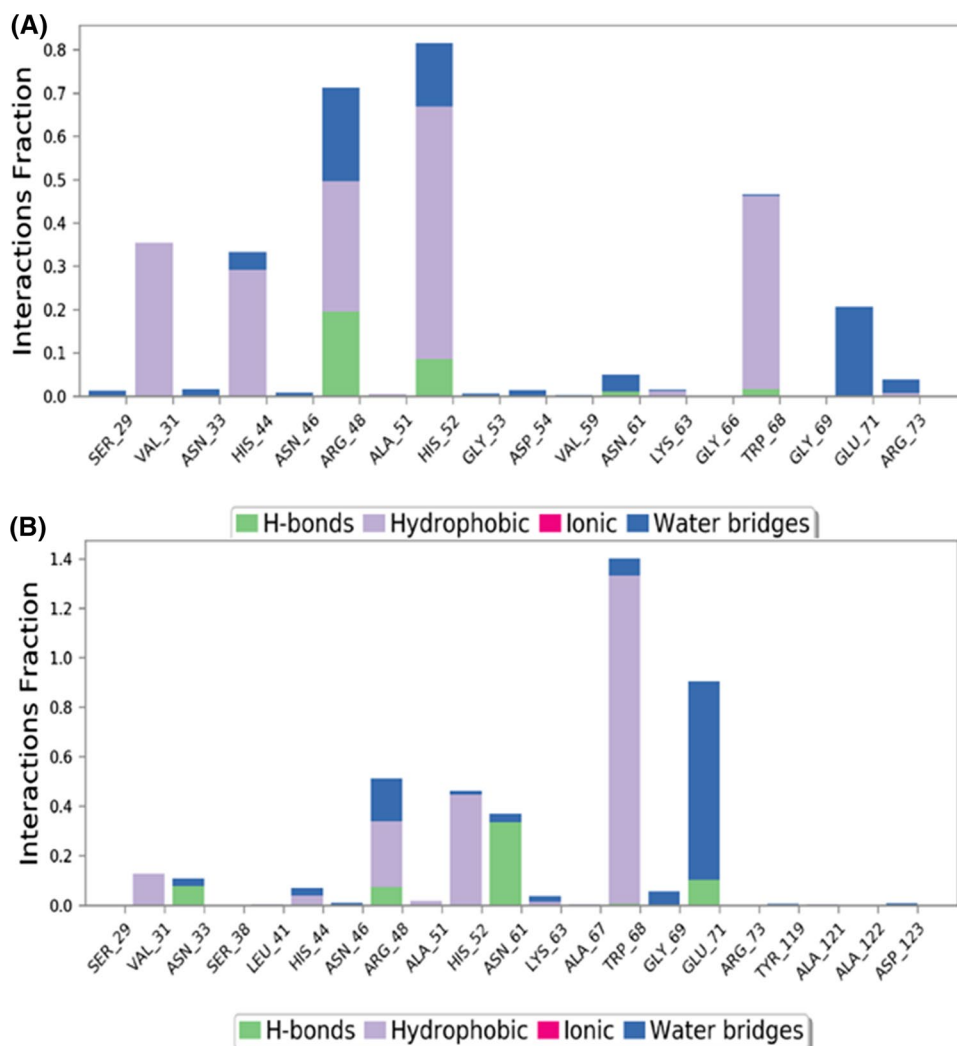
Experimental section

1.1 Chemistry

All the described starting materials, reagents and solvents in the current study were purchased from respective commercial suppliers. Analytical thin-layer chromatography (TLC) was performed on MERCK pre-coated silica gel 60-F254 aluminum plates. Visualization on TLC plates was achieved via UV light or in a few cases by iodine chamber. All melting points were recorded on Stuart[®] SMP30 melting point apparatus. Column chromatography was performed using silica gel (60–120 mesh) and was eluted with ethyl acetate-hexane mixture. NMR spectra were recorded on Bruker 500 (500 MHz for $^1\text{H NMR}$ and 125 MHz for $^{13}\text{C NMR}$) using DMSO as solvent. Chemical shift was reported in parts per million (ppm) with respect to internal standard Tetra Methyl Silane (TMS). Coupling constants were quoted in Hertz (Hz). High-resolution mass spectra (HRMS) were obtained on Agilent Q-TOF-Mass Spectrometer 6540-UHD LC/HRMS operating at 70 eV using direct inlet.

1.1 Synthetic protocol.

Fig. 8 Bar-chart representation of protein–ligand contacts of Gal-1 ligand complexes **a** 6i and **b** 7e during molecular dynamics simulation



Synthesis of 3-acetyl coumarin (**3**)

A mixture of salicylaldehyde (1 equiv.), ethyl acetoacetate (1 equiv.) and a few drops of piperidine were stirred at room temperature in neat conditions. Precipitation occurred almost immediately, and the reaction progress was monitored by TLC. After completion of the reaction, the reaction mixture was added into a beaker containing ice and stirred for 15 min. The precipitate thus obtained was then filtered and dried under vacuum. The obtained compound was recrystallized in absolute ethanol to yield compound **3**.

Synthesis of (E)-3-(3-(1H-indol-3-yl)acryloyl)-2H-chromen-2-one and methoxy derivative (**5a–b**)

Compound **3** (1 equiv.) was added to absolute ethanol with stirring, followed by the addition of simple indole-3-carboxaldehyde or methoxy-substituted derivative (1 equiv.). A catalytic amount of piperidine was then added, and the

reaction was continued at 70 °C for 2–3 h. The reaction progress was monitored by TLC. After completion of the reaction, the reaction mixture was added into a beaker containing ice and stirred vigorously. The precipitate thus obtained was then filtered under vacuum and recrystallized in absolute ethanol to yield compounds **5a** or **5b**.

General procedure for synthesis of N-substituted and unsubstituted indole-coumarin hybrids (**6a–n**, **7a–f**)

Compound **5a–b** (1 equiv.), obtained from above protocol, was added together with 1 equiv. of potassium carbonate in acetonitrile. Further, respective benzyl bromide or alkyl halides were added with constant stirring at room temperature. After completion of addition, the reaction was maintained at 70 °C for 3–4 h and the reaction progress was monitored by TLC. On completion, work-up was carried out or the acetonitrile was directly evaporated under reduced pressure to obtain the crude compound. The compounds were subjected

to column chromatography on silica gel to obtain the pure products.

4.3. Spectral data

1.1.1 (E)-3-(3-(1H-indol-3-yl)acryloyl)-2H-chromen-2-one (6a)

Yellow solid; 90% yield; mp: 200–202 °C; FT-IR (cm^{-1}): 3261, 1698, 1645, 1602; ^1H NMR (500 MHz, $\text{DMSO-}d_6$) δ 11.96 (s, 1H), 8.66 (s, 1H), 8.10–8.03 (m, 2H), 8.01–7.94 (m, 2H), 7.75 (t, $J=7.3$ Hz, 1H), 7.69 (d, $J=15.8$ Hz, 1H), 7.51 (dd, $J=11.6, 4.9$ Hz, 2H), 7.44 (t, $J=7.5$ Hz, 1H), 7.29–7.22 (m, 2H); ^{13}C NMR (125 MHz, $\text{DMSO-}d_6$) δ 186.60, 159.27, 154.81, 146.62, 140.18, 138.18, 134.85, 134.29, 130.74, 126.59, 125.36, 125.32, 123.39, 121.83, 120.73, 119.07, 118.99, 116.58, 113.44, 113.13; HRMS (ESI): m/z calcd for $\text{C}_{20}\text{H}_{13}\text{NO}_3$ 315.0895; found 316.0980 $[\text{M} + \text{H}]^+$.

1.1.1 (E)-3-(3-(1-methyl-1H-indol-3-yl)acryloyl)-2H-chromen-2-one (6b)

Yellow solid; 92% yield; mp: 210–212 °C; FT-IR (cm^{-1}): 3044, 1727, 1652, 1605; ^1H NMR (500 MHz, $\text{DMSO-}d_6$) δ 8.66 (s, 1H), 8.07 (s, 1H), 8.01 (t, $J=11.2$ Hz, 2H), 7.96 (dd, $J=7.7, 1.4$ Hz, 1H), 7.77–7.73 (m, 1H), 7.69 (d, $J=15.7$ Hz, 1H), 7.58 (d, $J=7.9$ Hz, 1H), 7.50 (d, $J=8.3$ Hz, 1H), 7.45–7.42 (m, 1H), 7.31 (ddd, $J=14.9, 13.9, 6.9$ Hz, 2H), 3.87 (s, 3H); ^{13}C NMR (125 MHz, $\text{DMSO-}d_6$) δ 186.46, 159.26, 154.82, 146.65, 139.39, 138.66, 137.94, 134.31, 130.75, 126.56, 125.88, 125.32, 123.44, 122.09, 120.76, 119.06, 118.95, 116.58, 112.40, 111.53, 33.55; HRMS (ESI): m/z calcd for $\text{C}_{21}\text{H}_{15}\text{NO}_3$ 329.1052; found 330.1152 $[\text{M} + \text{H}]^+$.

1.1.1 (E)-3-(3-(1-ethyl-1H-indol-3-yl)acryloyl)-2H-chromen-2-one (6c)

Yellow solid; 90% yield; mp: 202–204 °C; FT-IR (cm^{-1}): 2979, 1722, 1648, 1600; ^1H NMR (500 MHz, $\text{DMSO-}d_6$) δ 8.66 (s, 1H), 8.14 (s, 1H), 8.01 (t, $J=12.1$ Hz, 2H), 7.96 (dd, $J=7.8, 1.6$ Hz, 1H), 7.77–7.72 (m, 1H), 7.67 (d, $J=15.7$ Hz, 1H), 7.63 (dd, $J=7.6, 1.3$ Hz, 1H), 7.50 (d, $J=8.2$ Hz, 1H), 7.44 (td, $J=7.6, 1.2$ Hz, 1H), 7.30 (dddd, $J=14.8, 8.6, 7.2, 1.3$ Hz, 2H), 4.36–4.19 (m, 2H), 1.42 (t, $J=7.2$ Hz, 3H); ^{13}C NMR (125 MHz, $\text{DMSO-}d_6$) δ 186.56, 159.25, 154.81, 146.59, 139.51, 137.70, 136.41, 134.29, 130.73, 126.60, 126.07, 125.32, 123.41, 122.07, 120.89, 119.06, 118.99, 116.59, 112.59, 111.54, 41.39, 15.54; HRMS (ESI): m/z calcd for $\text{C}_{22}\text{H}_{17}\text{NO}_3$ 343.1208; found 344.1295 $[\text{M} + \text{H}]^+$.

1.1.1 (E)-3-(3-(1-benzyl-1H-indol-3-yl)acryloyl)-2H-chromen-2-one (6d)

Yellow solid; 89% yield; mp: 192–194 °C; FT-IR (cm^{-1}): 2920, 1715, 1652, 1600; ^1H NMR (500 MHz, $\text{DMSO-}d_6$) δ 8.64 (d, $J=18.0$ Hz, 1H), 8.27 (d, $J=20.0$ Hz, 1H), 8.07–7.99 (m, 2H), 7.96 (dd, $J=7.7, 1.3$ Hz, 1H), 7.77–7.72 (m, 1H), 7.71–7.66 (m, 1H), 7.62–7.58 (m, 1H), 7.51 (d, $J=7.3$ Hz, 1H), 7.43 (t, $J=11.2, 3.9$ Hz, 1H), 7.34 (dd, $J=9.3, 5.5$ Hz, 2H), 7.32–7.24 (m, 5H), 5.51 (s, 2H); ^{13}C NMR (125 MHz, $\text{DMSO-}d_6$) δ 186.67, 159.26, 154.82, 146.65, 139.30, 137.92, 137.57, 137.17, 134.31, 130.74, 129.17, 128.16, 127.69, 126.53, 126.17, 125.32, 123.57, 122.18, 120.92, 119.56, 119.05, 116.59, 112.96, 111.97, 50.02; HRMS (ESI): m/z calcd for $\text{C}_{27}\text{H}_{19}\text{NO}_3$ 405.1365; found 406.1428 $[\text{M} + \text{H}]^+$.

1.1.1 (E)-3-(3-(1-(4-bromobenzyl)-1H-indol-3-yl)acryloyl)-2H-chromen-2-one (6e)

Yellow solid; 86% yield; mp: 203–205 °C; FT-IR (cm^{-1}): 3044, 1717, 1650, 1602; ^1H NMR (500 MHz, $\text{DMSO-}d_6$) δ 8.66 (s, 1H), 8.25 (s, 1H), 8.01 (dt, $J=30.6, 11.4$ Hz, 3H), 7.75 (dd, $J=14.8, 7.1$ Hz, 1H), 7.71–7.63 (m, 1H), 7.59–7.56 (m, 1H), 7.52 (dd, $J=19.2, 8.0$ Hz, 3H), 7.43 (t, $J=7.3$ Hz, 1H), 7.29–7.19 (m, 4H), 5.50 (s, 2H); ^{13}C NMR (125 MHz, $\text{DMSO-}d_6$) δ 186.72, 159.23, 154.82, 146.65, 139.18, 137.82, 137.02, 137.01, 134.34, 132.08, 130.76, 129.92, 126.54, 126.19, 125.34, 123.65, 122.25, 121.31, 120.94, 119.72, 119.04, 116.60, 113.06, 111.91, 49.36; HRMS (ESI): m/z calcd for $\text{C}_{27}\text{H}_{18}\text{BrNO}_3$ 483.0470; found 486.0624 $[\text{M} + \text{H} + 2]^+$.

1.1.1 (E)-3-(3-(1-(3-chlorobenzyl)-1H-indol-3-yl)acryloyl)-2H-chromen-2-one (6f)

Yellow solid; 70% yield; mp: 206–208 °C; FT-IR (cm^{-1}): 3044, 1717, 1650, 1602; ^1H NMR (500 MHz, $\text{DMSO-}d_6$) δ 8.67 (s, 1H), 8.27 (s, 1H), 8.15–7.99 (m, 2H), 7.96 (d, $J=7.6$ Hz, 1H), 7.76 (dd, $J=14.7, 7.0$ Hz, 1H), 7.70 (d, $J=15.9$ Hz, 1H), 7.62 (dd, $J=9.3, 2.9$ Hz, 1H), 7.51 (dt, $J=14.7, 7.4$ Hz, 3H), 7.43 (dd, $J=13.8, 6.3$ Hz, 1H), 7.33–7.24 (m, 4H), 5.57 (s, 2H); ^{13}C NMR (125 MHz, $\text{DMSO-}d_6$) δ 186.76, 159.25, 154.83, 146.67, 140.36, 139.18, 137.82, 137.05, 134.35, 131.41, 131.09, 130.76, 130.45, 126.77, 126.54, 126.14, 125.35, 123.72, 122.37, 122.30, 120.97, 119.79, 119.05, 116.61, 113.11, 111.89, 49.24; HRMS (ESI): m/z calcd for $\text{C}_{27}\text{H}_{18}\text{ClNO}_3$ 450.0975; found 451.1292 $[\text{M} + \text{H}]^+$.

1.1.1 (E)-3-(3-(1-(3-methoxybenzyl)-1H-indol-3-yl)acryloyl)-2H-chromen-2-one (6g)

Yellow solid; 94% yield; mp: 213–215 °C; FT-IR (cm⁻¹): 2912, 1714, 1651, 1601; ¹H NMR (500 MHz, DMSO-*d*₆) δ 8.66 (s, 1H), 8.25 (s, 1H), 8.06–7.94 (m, 3H), 7.75 (t, *J*=7.7 Hz, 1H), 7.68 (d, *J*=15.8 Hz, 1H), 7.63–7.58 (m, 1H), 7.50 (d, *J*=8.3 Hz, 1H), 7.44 (t, *J*=7.4 Hz, 1H), 7.29–7.21 (m, 3H), 6.90–6.79 (m, 3H), 5.47 (s, 2H), 3.72 (s, 3H); ¹³C NMR (125 MHz, DMSO-*d*₆) δ 186.71, 159.93, 159.25, 154.82, 146.63, 139.32, 139.09, 137.95, 137.21, 134.32, 130.75, 130.32, 126.57, 126.13, 125.33, 123.58, 122.19, 120.91, 119.78, 119.56, 119.06, 116.60, 113.79, 113.25, 112.93, 111.99, 55.53, 49.95; HRMS (ESI): *m/z* calcd for C₂₈H₂₁NO₄ 435.1471; found 436.1526 [M+H]⁺.

1.1.1 (E)-3-(3-(1-(2-nitrobenzyl)-1H-indol-3-yl)acryloyl)-2H-chromen-2-one (6h)

Yellow solid; 82% yield; mp: 200–202 °C; FT-IR (cm⁻¹): 2923, 1720, 1644, 1604; ¹H NMR (500 MHz, DMSO-*d*₆) δ 8.67 (s, 1H), 8.22–8.15 (m, 2H), 8.09–8.02 (m, 2H), 7.97 (d, *J*=7.7 Hz, 1H), 7.74 (dd, *J*=15.8, 9.7 Hz, 2H), 7.68–7.55 (m, 2H), 7.52 (dd, *J*=17.3, 8.1 Hz, 2H), 7.44 (t, *J*=7.4 Hz, 1H), 7.29 (dt, *J*=15.0, 7.3 Hz, 2H), 6.59 (d, *J*=7.6 Hz, 1H), 5.93 (s, 2H); ¹³C NMR (125 MHz, DMSO-*d*₆) δ 186.78, 159.27, 154.85, 147.70, 146.74, 139.02, 138.19, 137.35, 134.91, 134.37, 133.41, 130.78, 129.36, 128.30, 126.52, 126.05, 125.68, 125.35, 123.88, 122.44, 121.01, 120.11, 119.06, 116.61, 113.46, 111.96, 47.68; HRMS (ESI): *m/z* calcd for C₂₇H₁₈FN₂O₃ 450.1216; found 451.1375 [M+H]⁺.

1.1.1 (E)-3-(3-(1-(4-fluorobenzyl)-1H-indol-3-yl)acryloyl)-2H-chromen-2-one (6i)

Yellow solid; 84% yield; mp: 218–220 °C; FT-IR (cm⁻¹): 3044, 1717, 1650, 1602; ¹H NMR (500 MHz, DMSO-*d*₆) δ 8.66 (s, 1H), 8.25 (s, 1H), 8.06–7.99 (m, 2H), 7.96 (dd, *J*=7.8, 1.7 Hz, 1H), 7.77–7.73 (m, 1H), 7.69 (d, *J*=15.7 Hz, 1H), 7.64–7.60 (m, 1H), 7.50 (d, *J*=8.4 Hz, 1H), 7.44 (t, *J*=7.5 Hz, 1H), 7.38–7.33 (m, 2H), 7.28 (dt, *J*=10.4, 3.5 Hz, 2H), 7.20–7.15 (m, 2H), 5.50 (s, 2H); ¹³C NMR (125 MHz, DMSO-*d*₆) δ 186.72, 163.05, 161.11, 159.25, 154.83, 146.64, 139.24, 137.81, 136.98, 134.32, 133.79, 133.77, 130.75, 129.94, 129.87, 126.56, 126.19, 125.33, 123.61, 122.22, 120.93, 119.65, 119.06, 116.60, 116.07, 115.90, 113.01, 111.94, 49.24; HRMS (ESI): *m/z* calcd for C₂₇H₁₈FNO₃ 423.1271; found 424.1348 [M+H]⁺.

1.1.1 (E)-3-(3-(1-(2-fluorobenzyl)-1H-indol-3-yl)acryloyl)-2H-chromen-2-one (6j)

Yellow solid; 86% yield; mp: 214–216 °C; FT-IR (cm⁻¹): 3051, 1718, 1654, 1603; ¹H NMR (500 MHz, DMSO-*d*₆) δ 8.66 (d, *J*=4.4 Hz, 1H), 8.23 (d, *J*=44.2 Hz, 1H), 8.04 (d, *J*=16.3 Hz, 2H), 7.95 (d, *J*=6.8 Hz, 1H), 7.71 (dd, *J*=16.6, 8.4 Hz, 2H), 7.62 (d, *J*=5.2 Hz, 1H), 7.49 (d, *J*=7.9 Hz, 1H), 7.45–7.41 (m, 1H), 7.38 (d, *J*=6.7 Hz, 1H), 7.29 (s, 2H), 7.25–7.19 (m, 1H), 7.15 (d, *J*=8.8 Hz, 1H), 7.10 (d, *J*=6.1 Hz, 1H), 5.55 (d, *J*=14.8 Hz, 2H); ¹³C NMR (125 MHz, DMSO-*d*₆) δ 186.78, 186.72, 159.25, 154.83, 146.68, 146.63, 139.25, 139.19, 137.85, 137.09, 134.33, 131.22, 130.75, 130.26, 126.55, 126.53, 126.03, 125.33, 123.75, 123.68, 122.26, 120.96, 119.78, 119.74, 119.06, 116.60, 114.68, 113.08, 111.90, 111.69, 49.41, 44.22; HRMS (ESI): *m/z* calcd for C₂₇H₁₈FN₂O₃ 423.1271; found 424.1348 [M+H]⁺.

1.1.1 (E)-3-(3-(1-(3,5-difluorobenzyl)-1H-indol-3-yl)acryloyl)-2H-chromen-2-one (6k)

Yellow solid; 85% yield; mp: 207–209 °C; FT-IR (cm⁻¹): 3046, 1717, 1649, 1601; ¹H NMR (500 MHz, DMSO-*d*₆) δ 8.67 (s, 1H), 8.28 (s, 1H), 8.03 (dd, *J*=12.3, 6.4 Hz, 2H), 7.96 (dd, *J*=7.7, 1.2 Hz, 1H), 7.77–7.69 (m, 2H), 7.63 (dd, *J*=6.0, 2.9 Hz, 1H), 7.50 (d, *J*=8.3 Hz, 1H), 7.44 (t, *J*=7.4 Hz, 1H), 7.33–7.27 (m, 2H), 7.17 (tt, *J*=9.3, 2.2 Hz, 1H), 7.02 (d, *J*=6.2 Hz, 2H), 5.54 (s, 2H); ¹³C NMR (125 MHz, DMSO-*d*₆) δ 186.72, 163.98, 163.88, 162.02, 161.91, 159.25, 154.83, 146.73, 142.09, 139.07, 137.78, 136.98, 134.35, 130.77, 126.49, 126.14, 125.33, 123.78, 122.35, 120.98, 119.90, 119.04, 116.60, 113.22, 111.82, 111.13, 110.93, 103.95, 103.75, 103.54, 49.10; HRMS (ESI): *m/z* calcd for C₂₇H₁₇F₂NO₃ 441.1176; found 442.1261 [M+H]⁺.

1.1.1 (E)-3-(3-(1-(2,5-difluorobenzyl)-1H-indol-3-yl)acryloyl)-2H-chromen-2-one (6l)

Yellow solid; 92% yield; mp: 211–213 °C; FT-IR (cm⁻¹): 3046, 1717, 1649, 1601; ¹H NMR (500 MHz, DMSO-*d*₆) δ 8.65 (s, 1H), 8.19 (s, 1H), 8.07–7.99 (m, 2H), 7.96 (d, *J*=7.5 Hz, 1H), 7.75 (t, *J*=7.6 Hz, 1H), 7.69 (d, *J*=15.8 Hz, 1H), 7.64 (d, *J*=7.6 Hz, 1H), 7.50 (d, *J*=8.3 Hz, 1H), 7.43 (t, *J*=7.3 Hz, 1H), 7.31 (dt, *J*=13.9, 6.8 Hz, 3H), 7.23 (d, *J*=7.8 Hz, 1H), 7.11 (s, 1H), 5.56 (s, 2H); ¹³C NMR (125 MHz, DMSO-*d*₆) δ 186.82, 159.24, 157.71, 157.59, 154.83, 146.66, 139.16, 137.80, 136.95, 134.34, 130.75, 129.97, 126.54, 126.01, 125.34, 123.77, 122.34, 120.99, 119.94, 119.05, 117.93, 117.87, 117.75, 117.67, 117.16,

117.09, 116.97, 116.89, 116.66, 116.60, 113.20, 111.63, 44.06, 4.15; HRMS (ESI): m/z calcd for $C_{27}H_{17}F_2NO_3$ 441.1176; found 442.1250 $[M+H]^+$.

1.1.1 (E)-3-(3-(1-(3,5-dimethylbenzyl)-1H-indol-3-yl)acryloyl)-2H-chromen-2-one (6m)

Yellow solid; 84% yield; mp: 210–212 °C; FT-IR (cm^{-1}): 2913, 1714, 1654, 1603; 1H NMR (500 MHz, DMSO- d_6) δ 8.66 (*s*, 1H), 8.22 (*s*, 1H), 8.06–7.93 (*m*, 3H), 7.79–7.72 (*m*, 1H), 7.68 (*d*, $J=15.7$ Hz, 1H), 7.59 (*d*, $J=8.7$ Hz, 1H), 7.51 (*t*, $J=7.4$ Hz, 1H), 7.47–7.41 (*m*, 1H), 7.29–7.26 (*m*, 2H), 6.91 (*s*, 3H), 5.41 (*s*, 2H), 2.21 (*s*, 6H); ^{13}C NMR (125 MHz, DMSO- d_6) δ 186.73, 159.26, 154.82, 146.60, 139.43, 138.25, 137.96, 137.38, 137.28, 134.32, 130.74, 129.64, 126.59, 126.11, 125.49, 125.34, 123.57, 122.17, 120.91, 119.49, 119.07, 116.60, 112.83, 111.98, 50.03, 21.35; HRMS (ESI): m/z calcd for $C_{29}H_{23}NO_3$ 433.1678; found 434.1766 $[M+H]^+$.

1.1.1 (E)-3-(3-(1-(4-methylbenzyl)-1H-indol-3-yl)acryloyl)-2H-chromen-2-one (6n)

yellow solid; 89% yield; mp: 200–202 °C; FT-IR (cm^{-1}): 2921, 1720, 1650, 1603; 1H NMR (500 MHz, DMSO- d_6) δ 8.66 (*s*, 1H), 8.24 (*s*, 1H), 8.07–7.92 (*m*, 3H), 7.73 (*d*, $J=6.7$ Hz, 1H), 7.68 (*d*, $J=15.7$ Hz, 1H), 7.59 (*d*, $J=2.7$ Hz, 1H), 7.49 (*d*, $J=7.7$ Hz, 1H), 7.43 (*s*, 1H), 7.26 (*s*, 2H), 7.19 (*d*, $J=7.0$ Hz, 2H), 7.13 (*d*, $J=7.0$ Hz, 2H), 5.44 (*s*, 2H), 2.24 (*s*, 3H); ^{13}C NMR (125 MHz, DMSO- d_6) 186.71, 159.24, 154.82, 146.58, 139.35, 137.89, 137.42, 137.11, 134.49, 134.30, 130.73, 129.70, 127.76, 126.60, 126.19, 125.33, 123.51, 122.14, 120.88, 119.51, 119.06, 116.60, 112.86, 112.00, 49.86, 21.12; HRMS (ESI): m/z calcd for $C_{28}H_{21}NO_3$ 419.1521; found 420.1595 $[M+H]^+$.

1.1.1 (E)-3-(3-(5-methoxy-1H-indol-3-yl)acryloyl)-2H-chromen-2-one (7a)

yellow solid; 92% yield; mp: 190–192 °C; FT-IR (cm^{-1}): 3196, 2988, 1715, 1641, 1601; 1H NMR (500 MHz, DMSO- d_6) δ 11.85 (*s*, 1H), 8.69 (*s*, 1H), 8.08–8.00 (*m*, 2H), 7.97 (*d*, $J=7.7$ Hz, 1H), 7.77–7.71 (*m*, 2H), 7.49 (*t*, $J=5.4$ Hz, 2H), 7.43 (*dd*, $J=14.9, 8.1$ Hz, 2H), 6.91 (*dd*, $J=8.8, 2.2$ Hz, 1H), 3.86 (*s*, 3H); ^{13}C NMR (125 MHz, DMSO- d_6) δ 186.14, 159.39, 155.59, 154.84, 146.79, 140.23, 134.92, 134.33, 133.01, 130.76, 126.42, 126.07, 125.32, 119.07, 118.51, 116.56, 113.80, 113.37, 112.83, 103.20, 55.90; HRMS (ESI): m/z calcd for $C_{21}H_{15}NO_4$ 345.1001; found 346.1080 $[M+H]^+$.

1.1.1 (E)-3-(3-(5-methoxy-1-methyl-1H-indol-3-yl)acryloyl)-2H-chromen-2-one (7b)

orange solid; 90% yield; mp: 195–197 °C; FT-IR (cm^{-1}): 3196, 2988, 1715, 1641, 1601; 1H NMR (500 MHz, DMSO- d_6) δ 8.69 (*s*, 1H), 7.99 (*dd*, $J=24.3, 9.4$ Hz, 2H), 7.91 (*m*, 1H), 7.73 (*d*, $J=15.4$ Hz, 1H), 7.69 (*m*, 1H), 7.49 (*m*, 3H), 7.44–7.41 (*m*, 1H), 6.96 (*d*, $J=7.9$ Hz, 1H), 3.86 (*s*, 3H), 3.83 (*s*, 3H); ^{13}C NMR (125 MHz, DMSO- d_6) δ 185.96, 159.39, 155.91, 154.86, 146.85, 139.45, 137.95, 134.35, 133.69, 130.79, 126.64, 126.40, 125.33, 119.08, 118.39, 116.57, 112.77, 112.34, 112.19, 103.32, 55.98, 33.72; HRMS (ESI): m/z calcd for $C_{22}H_{17}NO_4$ 359.1158; found 360.1277 $[M+H]^+$.

1.1.1 (E)-3-(3-(1-ethyl-5-methoxy-1H-indol-3-yl)acryloyl)-2H-chromen-2-one (7c)

yellow solid; 92% yield; mp: 192–194 °C; FT-IR (cm^{-1}): 3192, 2980, 1712, 1644, 1601; 1H NMR (500 MHz, DMSO- d_6) δ 8.68 (*d*, $J=4.3$ Hz, 1H), 8.08 (*d*, $J=4.3$ Hz, 1H), 8.02 (*dd*, $J=15.6, 4.5$ Hz, 1H), 7.98–7.95 (*m*, 1H), 7.73 (*dt*, $J=16.0, 6.3$ Hz, 2H), 7.57–7.48 (*m*, 3H), 7.47–7.40 (*m*, 1H), 6.96 (*d*, $J=10.1$ Hz, 1H), 4.28–4.19 (*m*, 2H), 3.87 (*d*, $J=4.6$ Hz, 3H), 1.49–1.35 (*m*, 3H); ^{13}C NMR (125 MHz, DMSO- d_6) δ 186.05, 159.37, 155.85, 154.85, 146.76, 139.55, 136.36, 134.31, 132.68, 130.76, 126.83, 126.43, 125.31, 119.08, 118.44, 116.56, 112.74, 112.38, 112.32, 103.43, 55.97, 41.55, 15.56; HRMS (ESI): m/z calcd for $C_{23}H_{19}NO_4$ 373.1314; found 374.1395 $[M+H]^+$.

1.1.1 (E)-3-(3-(1-benzyl-5-methoxy-1H-indol-3-yl)acryloyl)-2H-chromen-2-one (7d)

yellow solid; 89% yield; mp: 196–198 °C; FT-IR (cm^{-1}): 3196, 2988, 1723, 1647, 1601; 1H NMR (500 MHz, DMSO- d_6) δ 8.68 (*s*, 1H), 8.20 (*s*, 1H), 8.03 (*d*, $J=15.7$ Hz, 1H), 7.96 (*d*, $J=6.8$ Hz, 1H), 7.76–7.71 (*m*, 2H), 7.49 (*dd*, $J=7.5, 3.2$ Hz, 3H), 7.43 (*t*, $J=7.5$ Hz, 1H), 7.36–7.32 (*m*, 2H), 7.27 (*t*, $J=6.9$ Hz, 3H), 6.91 (*dd*, $J=8.9, 2.3$ Hz, 1H), 5.47 (*s*, 2H), 3.85 (*s*, 3H); ^{13}C NMR (125 MHz, DMSO- d_6) δ 186.20, 159.37, 155.89, 154.86, 146.82, 139.33, 137.61, 137.17, 134.35, 132.86, 130.78, 129.15, 128.14, 127.64, 126.96, 126.40, 125.32, 119.07, 119.02, 116.57, 112.91, 112.77, 112.72, 103.42, 55.96, 50.20. HRMS (ESI): m/z calcd for $C_{28}H_{21}NO_4$ 435.1471; found 436.1559 $[M+H]^+$.

1.1.1 (E)-3-(3-(1-(3-chlorobenzyl)-5-methoxy-1H-indol-3-yl)acryloyl)-2H-chromen-2-one (7e)

yellow solid; 82% yield; mp: 187–189 °C; FT-IR (cm^{-1}): 3192, 2981, 1724, 1646, 1603; 1H NMR (500 MHz, DMSO- d_6) δ 8.69 (*s*, 1H), 8.22 (*s*, 1H), 8.03 (*d*, $J=15.7$ Hz, 1H),

7.97 (*d*, $J=7.8$ Hz, 1H), 7.75 (*ddd*, $J=11.8, 4.5, 2.2$ Hz, 2H), 7.51 (*dd*, $J=7.6, 5.2$ Hz, 3H), 7.45–7.42 (*m*, 1H), 7.36 (*dd*, $J=3.9, 2.1$ Hz, 3H), 7.21 (*dd*, $J=6.5, 1.9$ Hz, 1H), 6.93 (*dd*, $J=8.9, 2.3$ Hz, 1H), 5.49 (*s*, 2H), 3.85 (*s*, 3H); ^{13}C NMR (125 MHz, $\text{DMSO-}d_6$) 186.25, 159.37, 155.96, 154.87, 146.86, 140.17, 139.20, 137.05, 134.37, 133.76, 132.75, 131.10, 130.79, 128.16, 127.51, 126.97, 126.38, 126.33, 125.34, 119.26, 119.07, 116.58, 113.04, 112.89, 112.68, 103.48, 55.98, 49.48; HRMS (ESI): m/z calcd for $\text{C}_{28}\text{H}_{20}\text{ClNO}_4$ 469.1081; found 470.1189 $[\text{M}+\text{H}]^+$.

1.1.1 (E)-3-(3-(1-(4-fluorobenzyl)-5-methoxy-1H-indol-3-yl)acryloyl)-2H-chromen-2-one (7f)

yellow solid; 92% yield; mp: 190–192 °C; FT-IR (cm^{-1}): 3192, 2980, 1723, 1648, 1603; ^1H NMR (500 MHz, $\text{DMSO-}d_6$) δ 8.69 (*d*, $J=4.8$ Hz, 1H), 8.33–8.12 (*m*, 1H), 8.03 (*dd*, $J=15.7, 2.3$ Hz, 1H), 7.97 (*d*, $J=7.7$ Hz, 1H), 7.74 (*dd*, $J=15.8, 8.1$ Hz, 2H), 7.50 (*dd*, $J=9.7, 4.4$ Hz, 3H), 7.46–7.41 (*m*, 1H), 7.38 (*dd*, $J=13.8, 7.3$ Hz, 1H), 7.28–7.21 (*m*, 1H), 7.20–7.06 (*m*, 2H), 6.97–6.88 (*m*, 1H), 5.49 (*t*, $J=23.1$ Hz, 2H), 3.85 (*s*, 3H); ^{13}C NMR (125 MHz, $\text{DMSO-}d_6$) 186.27, 159.38, 155.94, 154.86, 146.89, 146.84, 139.27, 139.22, 137.10, 134.36, 132.82, 132.76, 131.26, 131.19, 130.79, 130.63, 130.20, 126.95, 126.83, 126.38, 125.33, 125.27, 124.41, 123.70, 123.35, 119.24, 119.07, 116.58, 112.87, 103.46, 55.97, 49.59, 44.37; HRMS (ESI): m/z calcd for $\text{C}_{28}\text{H}_{20}\text{FNO}_4$ 453.1376; found 454.1532 $[\text{M}+\text{H}]^+$.

4.4. Biology

4.4.1. Quantikine ELISA human Gal-1 immunoassay

BT-474 cells were grown in 12-wellplate and treated with 20 μM concentration of compounds for 24 h. Then the supernatant was collected as Gal-1 is an extracellular secreted protein. Equal amounts of supernatant are subjected to Quantikine Enzyme-Linked Immunoassay (ELISA) as per manufacturer's protocol (DGAL 10, R&D systems). The supernatant was diluted twofold with calibrator diluent and incubated with human Gal-1-coated plates for 2 h at room temperature on a horizontal orbital microplate shaker and washed to remove any unbound protein. Gal-1-specific polyclonal antibody conjugated to horseradish peroxidase was added and incubated for 2 h on shaker. It was then washed and incubated with substrate solution for 30 min before terminating the reaction with 50 μl of stop solution. Amount of protein expression was detected at 450 nm using UV spectrophotometer.

4.4.2. Fluorescence measurements

In order to perform fluorescence binding studies of Gal-1 with compounds **6i** and **7e**, full length ORF of Gal-1 was cloned into pET28a expression vector followed by purification using Ni-NTA affinity chromatograph. Intrinsic fluorescence measurements were carried out on a Jasco spectrofluorimeter equipped with peltier at 25 °C. Compounds **6i** and **7e** were dissolved in DMSO to prepare a stock of 10 mM and were used in the range of 0–65 μM . Purified Gal-1 with concentration of 13 μM in 10 mM phosphate buffer (pH 7.5) was excited at 280 nm, and the emission was recorded from 300 to 400 nm using a cuvette of 10 mm path length. Slit width 5 nm was used for excitation and emission, while scan speed was maintained at 100 nm/min. Buffer correction was made for each spectrum. Binding constant (K_a) and number of binding sites (n) were determined using modified Stern–Volmer equation, i.e., $\log(F_0 - F)/F = \log K_a + n \log [Q]$ where F_0 and F are the intensity of the protein in the absence and presence of the ligand, respectively, whereas n is the number of binding sites and Q is the ligand concentration.

Computational studies

Molecular docking

Compounds **6i** and **7e** were sketched by using the 2D-sketcher in Maestro (Schrodinger Suite 2020–2). These two compounds were then prepared using the “LigPrep” module by generating low-energy ionization and tautomeric states with a pH of 7.4 using OPLS-2005 force field for minimization. The molecular docking studies for the prepared compounds were performed using the Glide module in Maestro Schrodinger Suite 2020–2. The three-dimensional crystal structure of the target protein Gal-1 with the PDB ID: 4Y24 was retrieved from Protein Data Bank, PDB. First, the retrieved protein was prepared using the “Protein preparation wizard.” The protein was imported and pre-processed to assign the bond orders and add hydrogen. All the water molecules were deleted followed by optimization and minimization by using OPLS-2005 force field. Next, a grid was generated around the co-crystal of the prepared protein by “Receptor grid generation.” The grid generation was performed to define the active site of the protein. The region was enclosed in a box size of $10 \times 10 \times 10$ Å. The prepared compounds were then docked at the active site using Glide XP flexible ligand docking. Van der Waals radius was maintained < 0.8 . The scoring function and the protein–ligand interactions were further analyzed.

4.5.2. Molecular dynamics simulation and MM-GBSA calculations

In order to more precisely evaluate the protein and the ligand interactions, MD simulations of 30 ns were performed for **6i** and **7e** using Desmond module of Schrödinger suite (2020–2). Aqueous biological system was built by using OPLS_2005 force field, and TIP3P model was used to simulate the water molecules. Orthorhombic periodic boundary conditions were set up to specify the shape and size of the repeating unit buffered at 10 Å distances. The physiological pH was neutralized by adding 0.15 M NaCl. 300 K temperature and 1.01325 bar pressure was maintained by using Nose–Hoover temperature coupling and Martina–Tobias–Klein method for the constant pressure, respectively. Reversible reference system propagation algorithm (REPSA), a time stepping algorithm, was used for near non-bonded (2 fs), far non-bonded (6 fs) and bonded interactions (2 fs). In the end, molecular dynamics simulations (30 ns) were performed for the two ligands.

The MM/GBSA method (Schrödinger Release 2020–2: Prime, Schrödinger, LLC, New York, NY, 2020–2) was used to calculate the binding free energy (ΔG_{bind}), for receptor–binder complex systems.

Supplementary Information The online version supplementary material available at <https://doi.org/10.1007/s11696-021-01534-w>.

Acknowledgements Authors are thankful to DoP, Ministry of Chemicals and Fertilizers, Govt. of India, New Delhi, for the award of NIPER fellowship and supporting the work.

Funding The research carried out received no external funding.

Compliance with ethical standards

Conflict of interest The authors declare that they have no conflict of interest.

References

- Barondes SH, Cooper DN, Gitt MA, Leffler H (1994) Galectins. Structure and function of a large family of animal lectins. *J Biol Chem* 269(33):20807–20810
- Blanchard H, Bum-Erdene K, Bohari MH, Yu X (2016) Galectin-1 inhibitors and their potential therapeutic applications: a patent review. *Expert Opin Ther Pat* 26(5):537–554. <https://doi.org/10.1517/13543776.2016.1163338>
- Boltje TJ, Buskas T, Boons GJ (2009) Opportunities and challenges in synthetic oligosaccharide and glycoconjugate research. *Nat chem* 1(8):611–622. <https://doi.org/10.1038/nchem.399>
- Cooper DN, Barondes SH (1990) Evidence for export of a muscle lectin from cytosol to extracellular matrix and for a novel secretory mechanism. *J Cell Biol* 110(5):1681–1691. <https://doi.org/10.1083/jcb.110.5.1681>
- Di-Lella S, Ma L, Diaz Ricci JC, Rabinovich GA, Asher SA, Álvarez RM (2009) Critical role of the solvent environment in galectin-1 binding to the disaccharide lactose. *Biochemistry* 48(4):786–791. <https://doi.org/10.1021/bi801855g>
- Gabr M, Rehman AU, Chen HF (2020) A quinoline-pyrazole scaffold as a novel ligand of galectin-3 and suppressor of trem2 signaling. *ACS Med Chem Lett*. <https://doi.org/10.1021/acsmchemlett.0c00330>
- Gomes MN, Muratov EN, Pereira M, Peixoto JC, Rosseto LP, Cravo PV, Andrade CH, Neves BJ (2017) Chalcone derivatives: promising starting points for drug design. *Molecules* 22(8):1210. <https://doi.org/10.3390/molecules22081210>
- Gomtsyan A (2012) Heterocycles in drugs and drug discovery. *Chem Heterocycl Comp* 48(1):7–10. <https://doi.org/10.1007/s10593-012-0960-z>
- Goud NS, Ghouse MS, Vishnu J, Pranay J, Alvala R, Talla V, Qureshi IA, Alvala M (2019a) Synthesis and biological evaluation of novel heterocyclic imines linked coumarin-thiazole hybrids as anticancer agents. *Curr Med Chem: Anti-Cancer Agents* 19(4):557–566. <https://doi.org/10.2174/1871520619666190207140120>
- Goud NS, Ghouse SM, Vishnu J, Komal D, Talla V, Alvala R, Pranay J, Kumar J, Qureshi IA, Alvala M (2019b) Synthesis of 1-benzyl-1H-benzimidazoles as galectin-1 mediated anticancer agents. *Bioorg Chem* 89:103016. <https://doi.org/10.1016/j.bioorg.2019.103016>
- Goud NS, Makani VK, Pranay J, Alvala R, Qureshi IA, Kumar P, Bharath RD, Nagaraj C, Yerramsetty S, Pal-Bhadra M, Alvala M (2020) Synthesis, 18F-radiolabeling and apoptosis inducing studies of novel 4,7-disubstituted coumarins. *Bioorg Chem* 97:103663. <https://doi.org/10.1016/j.bioorg.2020.103663>
- He J, Baum LG (2006) Galectin interactions with extracellular matrix and effects on cellular function. *Methods Enzymol* 417:247–256. [https://doi.org/10.1016/S0076-6879\(06\)17017-2](https://doi.org/10.1016/S0076-6879(06)17017-2)
- Hughes RC (1999) Secretion of the galectin family of mammalian carbohydrate-binding proteins. *Biochim Biophys Acta* 1473(1):172–185. [https://doi.org/10.1016/S0304-4165\(99\)00177-4](https://doi.org/10.1016/S0304-4165(99)00177-4)
- Kurt BZ, Kandas NO, Dag A, Sonmez F, Kucukislamoglu M (2020) Synthesis and biological evaluation of novel coumarin-chalcone derivatives containing urea moiety as potential anticancer agents. *Arab J Chem* 13(1):1120–1129. <https://doi.org/10.1016/j.arabj.2017.10.001>
- Lakowicz JR (2013) Principles of fluorescence spectroscopy. Springer, New York
- Leffler H, Carlsson S, Hedlund M, Qian Y, Poirier F (2002) Introduction to galectins. *Glycoconj J* 19(7–9):433–440. <https://doi.org/10.1023/B:GLYC.0000014072.34840.04>
- Liu FT, Patterson RJ, Wang JL (2002) Intracellular functions of galectins. *Biochim Biophys Acta* 1572(2–3):263–273. [https://doi.org/10.1016/S0304-4165\(02\)00313-6](https://doi.org/10.1016/S0304-4165(02)00313-6)
- Mercier S, St-Pierre C, Pelletier I, Ouellet M, Tremblay MJ, Sato S (2008) Galectin-1 promotes HIV-1 infectivity in macrophages through stabilization of viral adsorption. *Virology* 371(1):121–129. <https://doi.org/10.1016/j.virol.2007.09.034>
- Meynier C, Feracci M, Espeli M, Chaspoul F, Gallice P, Schiff C, Guerlesquin F, Roche P (2009) NMR and MD investigations of human galectin-1/oligosaccharide complexes. *Biophys J* 97(12):3168–3177. <https://doi.org/10.1016/j.bpj.2009.09.026>
- Patterson RJ, Wang W, Wang JL (2004) Understanding the biochemical activities of galectin-1 and galectin-3 in the nucleus. *Glycoconj J* 19:499–506. <https://doi.org/10.1023/B:GLYC.0000014079.87862.c7>
- Pires DE, Blundell TL, Ascher DB (2015) pkCSM: predicting small-molecule pharmacokinetic and toxicity properties using graph-based signatures. *J Med Chem* 58(9):4066–4072. <https://doi.org/10.1021/acs.jmedchem.5b00104>

- Rabinovich GA (2005) Galectin-1 as a potential cancer target. *Br J Cancer* 92(7):1188–1192. <https://doi.org/10.1038/sj.bjc.6602493>
- Rajput VK, Leffler H, Nilsson UJ, Mukhopadhyay B (2014) Synthesis and evaluation of iminocoumaryl and coumaryl derivatized glycosides as galectin antagonists. *Bioorg Med Chem Lett* 24(15):3516–3520. <https://doi.org/10.1016/j.bmcl.2014.05.063>
- Rajput VK, MacKinnon A, Mandal S, Collins P, Blanchard H, Leffler H, Sethi A, Schambye H, Mukhopadhyay B, Nilsson UJ (2016) A selective galactose–coumarin-derived galectin-3 inhibitor demonstrates involvement of galectin-3-glycan interactions in a pulmonary fibrosis model. *J Med Chem* 59(17):8141–8147. <https://doi.org/10.1021/acs.jmedchem.6b00957>
- Sethi A, Joshi K, Sasikala K, Alvala M (2019) Molecular docking in modern drug discovery: principles and recent applications. *IntechOpen, Drug Discov Adv*. <https://doi.org/10.5772/intechopen.85991>
- Sethi A, Sanam S, Munagalasetty S, Jayanthi S, Alvala M (2020) Understanding the role of galectin inhibitors as potential candidates for SARS-CoV-2 spike protein: in silico studies. *RSC Adv* 10(50):29873–29884. <https://doi.org/10.1039/D0RA04795C>
- Sravanthi TV, Manju SL (2016) Indoles—a promising scaffold for drug development. *Eur J Pharm Sci* 91:1. <https://doi.org/10.1016/j.ejps.2016.05.025>
- Sundblad V, Morosi LG, Geffner JR, Rabinovich GA (2017) Galectin-1: a jack-of-all-trades in the resolution of acute and chronic inflammation. *J Immunol* 199(11):3721–3730. <https://doi.org/10.4049/jimmunol.1701172>
- Tejler J, Leffler H, Nilsson UJ (2005) Synthesis of O-galactosyl aldoximes as potent LacNAc-mimetic galectin-3 inhibitors. *Bioorg Med Chem Lett* 15(9):2343–2345. <https://doi.org/10.1016/j.bmcl.2005.02.079>
- Tejler J, Salameh B, Leffler H, Nilsson UJ (2009) Fragment-based development of triazole-substituted O-galactosyl aldoximes with fragment-induced affinity and selectivity for galectin-3. *Org Biomol Chem* 7(19):3982–3990. <https://doi.org/10.1039/B909091F>
- Thijssen VL, Heusschen R, Caers J (2015) Griffioen AW (2015) Galectin expression in cancer diagnosis and prognosis: a systematic review. *Biochim Biophys Acta* 1855(2):235–247. <https://doi.org/10.1016/j.bbcan.2015.03.003>
- Vitaku E, Smith DT, Njardarson JT (2014) Analysis of the structural diversity, substitution patterns, and frequency of nitrogen heterocycles among us FDA approved pharmaceuticals: miniperspective. *J Med Chem* 57(24):10257–10274. <https://doi.org/10.1021/jm501100b>
- Wada M, Ono S, Kadoya T, Kawanami T, Kurita K, Kato T (2003) Decreased galectin-1 immunoreactivity of the skin in amyotrophic lateral sclerosis. *J Neurol Sci* 208(1–2):67–70. [https://doi.org/10.1016/S0022-510X\(02\)00424-0](https://doi.org/10.1016/S0022-510X(02)00424-0)
- Zhuang C, Zhang W, Sheng C, Zhang W, Xing C, Miao Z (2017) Chalcone: a privileged structure in medicinal chemistry. *Chem Rev* 117(12):7762–7810. <https://doi.org/10.1021/acs.chemrev.7b00020>

Publisher's Note Springer Nature remains neutral with regard to jurisdictional claims in published maps and institutional affiliations.

Authors and Affiliations

Aaftaab Sethi¹ · K. Sasikala¹ · Pranay Jakkula² · Divya Gadde³ · Swetha Sanam¹ · Insaf A. Qureshi² · Venu Talla³ · Mallika Alvala^{1,4} 

¹ Department of Medicinal Chemistry, National Institute of Pharmaceutical Education and Research (NIPER), Hyderabad 500037, India

² Department of Biotechnology and Bioinformatics, School of Life Sciences, University of Hyderabad, Hyderabad 500046, India

³ Department of Pharmacology and Toxicology, National Institute of Pharmaceutical Education and Research (NIPER), Hyderabad 500037, India

⁴ MARS Training Academy, Hyderabad, India